Stretchable, Soft and Wearable Polymeric Heaters and Strain Sensors Fabricated using Liquid Metals

Sihyun Kim[a,b], Masato Saito[c], Yuwen Wei[a,b], Priyanuj Bhuyan[a,b], Minjae Choe[a,b], Toshinori Fujie[c], Kunal Mondal[d,e,f], Sungjune Park[a,b]

[a]*Department of Nano Convergence Engineering, Jeonbuk National University, 54896, Jeonju, Korea*
[b]*Department of PolymerNano Science and Technology, Jeonbuk National University, 54896, Jeonju, Korea*
[c]*School of Life Science and Technology, Tokyo Institute of Technology, B50, 4259 NagatsutaCho, Midoriku, 2268501, Yokohama, Japan*
[d]*Materials Science and Engineering Department, Idaho National Laboratory, ID, 83415, Idaho Falls, USA*
[e]*Department of Civil & Environmental Engineering, Idaho State University, Pocatello, ID 83209, USA*
[f]*The Fusion and Fission Energy and Science Directorate, Oak Ridge National Laboratory, 1 Bethel Valley Road, Oak Ridge, TN 37830, USA*

Abstract

Wearable electronic devices (WEDs) are receiving significant attention because of the increasing interest in soft robotics, electronic skin, and wearable sensors. Liquid metals (LMs) are compelling for WEDs owing to their metallic conductivity, fluidic nature, and low toxicity. Herein, we fabricated stretchable and soft WEDs using LM (eutectic gallium-indium alloy) wires (LMWs) patterned via force wetting through custom-made stencils on an elastic substrate. LMWs can generate thermal energy via Joule heating upon current application and deliver it to the substrate, resulting in wearable polymeric heaters. The LM mixed with carbonyl iron particles (CIPs) can also be patterned while preserving fluidic behavior. The degree of thermal energy generated through the LMWs can be manipulated as a function of the CIP concentration in the LM and geometrical factors of the electrode patterns, i.e., width and length. An elastic film patterned with LMWs attached to the human body exhibits changes in the effective electrical resistance depending on applied strain, demonstrating potential as a wearable strain sensor. This LM utilized WED that can generate thermal energy upon current application through the LMWs and detect the bodily motion has significant potential for application in wearable thermotherapy, electronic skin, and soft sensors.

Keywords: Liquid metal, Stretchable and soft electronics, Wearable polymeric heater, Strain sensor

1. Introduction

Wearable electronic devices (WEDs) have received considerable attention owing to the growing interest in soft robotics [1–3], biomedical treatments [4–7], electronic skin [8–11], wireless communication [12], and conformable sensors [13–15]. WEDs are typically manufactured using elastic polymers as matrix incorporated with conductive fillers to establish electrical pathways [16–18]. Underlying principle for wearable devices is preserving electrical conductivity when strained and changing the electrical behavior in response to external stimuli.

WEDs are promising for application in wearable thermotherapy because they can be attached to curved surfaces while maintaining electrical operation during deformation and

can generate thermal energy while adhered to the human body [19–24]. WEDs can also exhibit changes in electrical resistance in response to external stimuli, which is useful for creating wearable strain sensors. Despite this unique feature, the degree of freedom for deformation of the devices may remain limited by electrode rigidity. Although previous studies have demonstrated the creating stretchable electrodes by utilizing unique geometric features (zigzag and corrugated patterns) [19,22,25–27], intrinsically fluidic conductors are compelling because they are highly deformable while retaining electrical conductivity.

Gallium-based liquid metal (LM) (eutectic gallium indium (EGaIn)) that remains in a liquid state at room temperature because of its low melting point (~15.5 ˚C) is a promising electrode for WEDs owing to its metallic conductivity, fluidic behavior, and low toxicity [28–31]. These features can allow the LM to overcome limitations of conventional devices fabricated using rigid metals such as restriction of deformation. [29] The LM can adhere to various substrates because of a thin oxide layer (~3 nm) spontaneously formed on its surface in the air [29,30]. This allows the metal to be patterned onto substrates in desired shapes using unconventional methods, including vacuum-assisted filing [32], laser patterning [33,34], direct writing [35,36], and stencil printing via forced wetting [37]. Recently, liquid metal wires (LMWs) patterned into thermochromic elastic polymers have been shown to generate thermal energy upon current application to the wires. Once thermal energy is generated, it is delivered to the polymers, resulting in a color change of thermochromic polymers [38–40]. Additionally, heterogeneous metal or silica fillers incorporated into the LM can increase the resistance, allowing for enhanced thermal energy generation [41,42].

Herein, we report soft and stretchable WEDs that can be used for wearable heaters and strain sensors consisting of LM composite electrodes formed by mixing LM with carbonyl iron particles (CIPs) (LM@CIP). The addition of CIPs to LM aids oxide layer promotion which is vital for two important phenomenon: first being adhesion of electrode material to the elastomeric substrate, i.e., when LM@CIP is patterned on the elastic substrate via forced wetting through dedicated stencils, it firmly adheres on the substrate through the oxide layer on the LM surface; and second being increase in resistance of the electrode material leading to superior joule heating effect as compared to that of pure LM. The preservation of fluidic behavior, even after mixing with CIPs, allows the LM@CIP composites to be patterned by unconventional approach identically. The thermal behavior of the LMWs was characterized by observing their Joule heating phenomenon through application of current while varying certain parameters, viz., the CIP concentration, applied electrical currents, and electrode pattern geometries.

We used a non-crosslinked polysiloxane elastomer with a high resilience due to highly entangled polymeric chains as a substrate, thus, the thermal properties of the polymeric heater containing the LM electrode showed excellent dynamic stability. The WED showed 4.8% variation in the generated thermal energy when a strain of 50% was applied which is exceptionally smaller than that of previously reported stretchable heaters at similar strains [19,21,25,43–46](Table 1). For instance, Zhou et al. reported a stretchable heater using conductive polymers that showed a variation in heating temperature of 10% at 30% strain [43]. Wang et al. prepared a stretchable heater using graphene fibers with variation in heating temperature of 85.9% at 33% strain [25]. In addition, the WEDs developed in this work exhibit ultrasoftness (Young's modulus of 116 kPa), ultrastretchability (elongation at break of > 1300%) and strong adhesion to the surfaces, thereby demonstrating high

motion sensing ability under external strain when attached to human joints, including the finger, wrist, and elbow. The WED prepared herein utilizing the LM electrode would be well-suited for application in soft robotics and devices for biomedical treatments including hypothermia and wearable strain sensors.

Table 1
Comparisons with the other wearable heating devices reported in the literatures.

Materials	Degree of strain	Temperature variation	Ref.
Ligand-exchanged Ag nanowire	50%	12.18%	[19]
Ag nanowire	30%	37.50%	[21]
Graphene fibers	33%	85.90%	[25]
PEDOT:PSS	30%	10%	[43]
PET/Ag nanowire/PDMS	40%	45.45%	[44]
Cupper nanowire	40%	13.20%	[46]
LM@CIP	50%	4.8%	This work

2. Materials and Methods

2.1. Preparation of LM composites mixed with CIPs

To prepare LM composites mixed with CIP (LM@CIP), the LM (EGaIn, 75.5% Ga and 24.5% In by weight, Indium Corporation, Clinton, NY, USA) was treated by dropping 6 M HCl onto the LM in a petri dish to remove the oxide layer. Subsequently, the CIPs with a diameter of 5–9 μm (Sigma-Aldrich, St. Louis, MO, USA) were added to the LM to form composites with concentrations ranging from 10 to 40 wt% [47,48]. Once mixed with a permanent magnet (NdFeB, 35 N grade, 50x10x5 mm^3) placed below the petri dish, HCl was removed using a cotton swab, and the composite was dried in an oven at 60 ˚C for 10 min. A schematic of the LM@CIP fabrication process is shown in Figure 1a.

2.2. Fabrication of WEDs patterned with LM

Figure 1b shows a schematic of the fabrication process for LMWs using stencil method. LMWs are fractally patterned on stretchable and elastic substrates using two commercial silicone elastomers (Ecoflex 00-30, Smooth-on, Macungie, PA, USA and Exsil-100, Gelest, Morrisville, PA, USA). Once the stencil was created on a polyethylene terephthalate (PET) film using a stencil printer (Cameo 4, Silhouette America Inc., Lindon, UT, USA), the LM and LM@CIP were patterned through the dedicated PET stencil using a paint brush onto the silicone elastomer substrates thermally cured at 80 ˚C for 4 h. Once the stencil mask was removed, the electrode was covered with the freshly prepared silicone elastomer using a film applicator (Elcometer 3580, Elcometer, Manchester, UK), followed by thermal curing. Copper wires were connected to the ends of the LM electrodes to apply an electrical current. A schematic of the device fabrication is shown in Figure 1c.

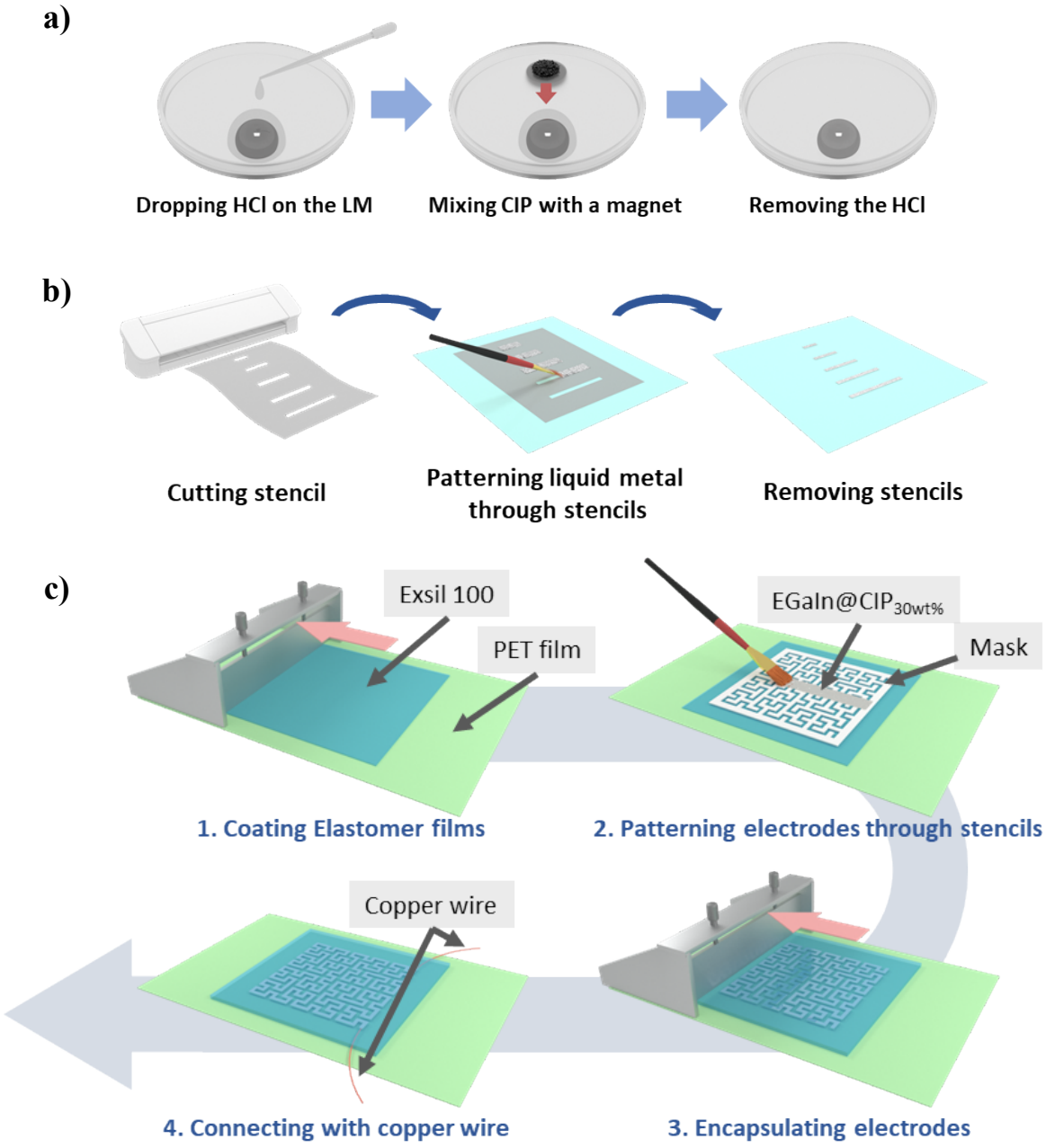

Figure 1: Schematic of the fabrication process of (a) LM@CIP, (b) LMWs on an elastic substrate, and (c) WED by patterning LMWs via forced wetting followed by encapsulating the LMWs.

2.3. *Characterization*

The electrical properties of the LMWs patterned in the WEDs were measured using a benchtop multimeter (34461A, Keysight Technologies, Santa Rosa, California, USA), and thermal properties were measured using an IR camera (FLIR C3, FLIR, Wilsonville, Oregon, USA). FLIR tools were used to analyze the thermal images. Current was applied through the LMWs using a direct current power supply (LW-K305D, Longwei Instrument Co., Ltd.,

Guangdong, China) to characterize heat generation performance. The surface topographies and constituent elements of the LM@CIP wires were characterized using scanning electron microscopy (SEM; SUPRA40VP, Carl Zeiss AG, Oberkochen, Germany) and energy dispersive spectrometry (EDS; Ultim Max 100, Oxford Instruments, Abingdon, UK), respectively. To characterize the effective resistance changes upon repeated constant strains, an extensometer (Quasar 2.5 single column, Galdabini, Cardano al Campo, Italy) with a 1 kN load cell and a deformation rate of 10 mm min^{-1} was used

3. Results and Discussion

As shown in Figure 1, LM and LM@CIP were patterned to form wires on elastic substrates via forced wetting through a stencil. LM@CIP was prepared by removing the oxide layer with HCl on the LM and subsequently mixing the LM with CIPs. The HCl can effectively remove the oxide layer from the surface of LM and enable iron particles react with gallium by galvanic replacement reaction. (Figure 1a and Video S1) [47,48]. LM@CIP preserved the fluidic properties and possessed surface oxides, allowing for the wire patterning via forced wetting through the stencils (Figure 1b and c). This facile method allows the preparation of wires with various geometries straightforwardly (Figure S1). Notably, the surface morphologies of LM@CIP differ with the CIP concentration. As the LM@CIP has a higher CIP concentration, paste-like morphologies are formed due to the solid fillers as observed by further oxidizing and pressuring the LM@CIP (Figure S2).

Figure 2 shows the thermal energy generated by applying a current through the LMWs and relative resistance of the LMWs with various CIP contents, geometries (length and width), and applied strains. The thermal energy generated upon current application through the LM wires can be predicted using Equation (1).

$$P = I^2R \tag{1}$$

where P, I, and R indicate the thermal energy generated, applied current through the LM electrodes, and LM electrode resistance, respectively. The LM electrode resistance can be expressed using Equation (2).

$$R = \rho\frac{L}{A} \tag{2}$$

where ρ, L, and A are the bulk resistance, length, and cross-sectional area, respectively. Combining Equations (1) and (2), the thermal energy generated by Joule heating can be expressed using Equation (3).

$$P = I^2\rho\frac{L}{A} \tag{3}$$

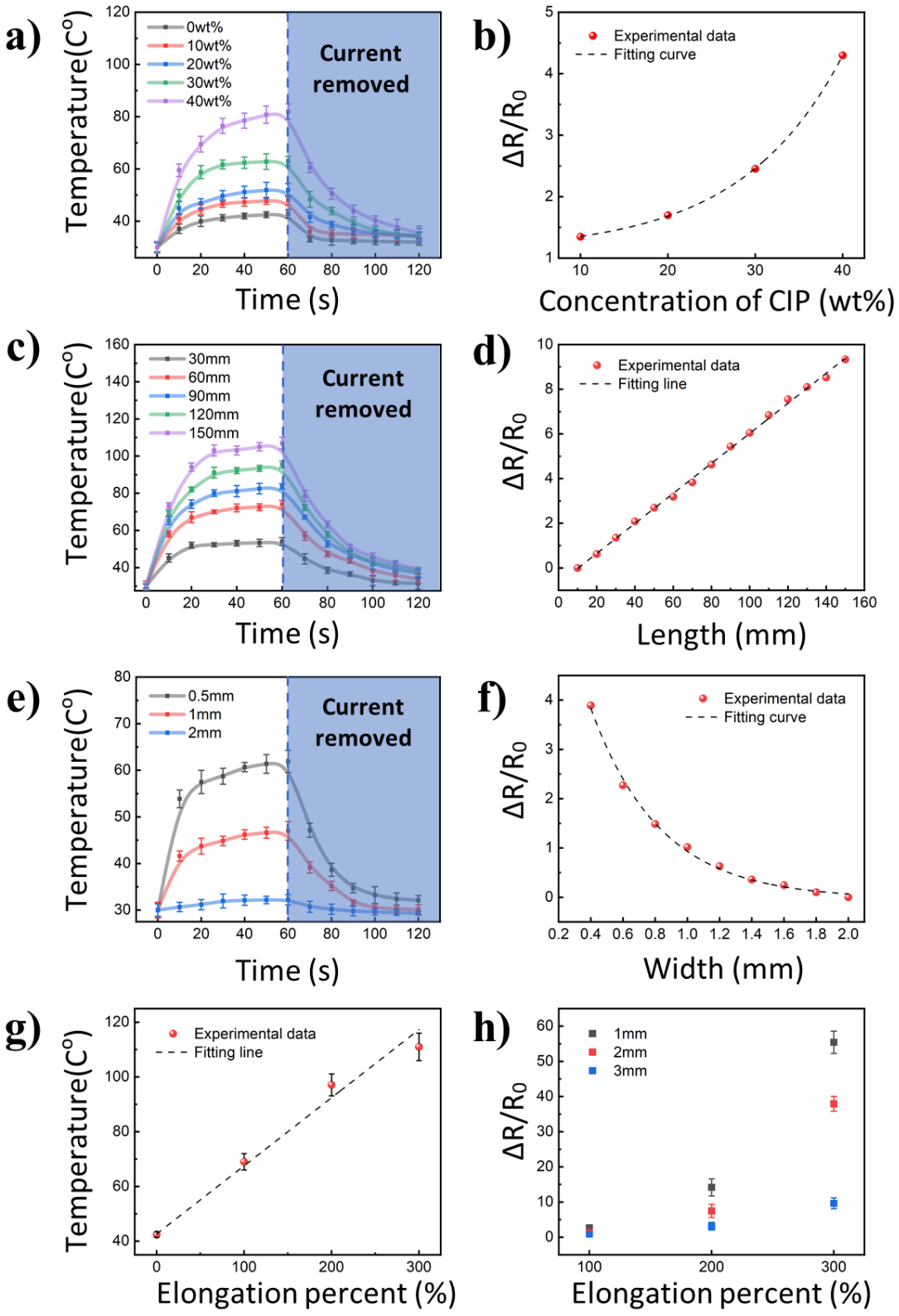

Figure 2: (a, c, e, g) Characterization of thermal energy generated via Joule heating through the LM wires and LM@CIP wires. (b, d, f, h) Relative resistance of the wires with various (a,b) CIP contents, (c,d) wire lengths, (e,f) wire widths, and (g,h) applied strains.

As shown in Figure 2a, the thermal energy generated by applying a current of 1 A through the LMWs with a width of 3 mm and length of 150 mm increases as a function of the CIP concentration in the range of 0–40 wt%. With higher CIP contents in the LMWs, the oxide layer area increases, resulting in increased resistance (Figure 2b). Although the ability of LM@CIP to generate a high thermal energy increased as a function of CIP concentration, the LM@CIP with 30 wt% CIP was used for further characterizations because this threshold ratio can preserve fluidic behavior to pattern by forced wetting through the stencils. Figure 2c and d show the thermal energy and relative resistance generated by applying a current of 1 A through the LM@CIP wires (30 wt% CIP) with a width of 2 mm and various lengths ranging from 30 to 150 mm. The individual maximum temperatures of the LMWs reached increase as a function of the wire length (Figure 2c) because of the increased resistance (Figure 2d). Figure 2e shows that the thermal energy generated by applying a current of 0.5 A through the LM@CIP wires with a length of 150 mm inversely increases as a function of width because the effective resistance decreases as the width of the electrodes increases (Figure 2f). When the current is removed, the LMWs recover their initial temperatures. Figure 2g shows the changes in maximum temperatures of the LM@CIP wires with various degrees of strain while applying a current of 1 A for 60 seconds through wires with a width of 3 mm and length of 30 mm. The LMWs generated a higher thermal energy as a function of strain because the geometric width of the LMWs decreases, whereas the length increases upon strain application (Figure S3). Figure 2h shows the relative resistance of the LM@CIP wires with various widths upon strain application. The LM@CIP wires exhibit the effective resistances increased as a function of strain, and the values inversely increase with the wire width. Notably, the characterization of thermal energy generated by applying current through the LM electrodes and the change in the relative resistance of the electrodes with geometric widths and lengths follow the theoretical expectation, as shown in Equations (2) and (3).

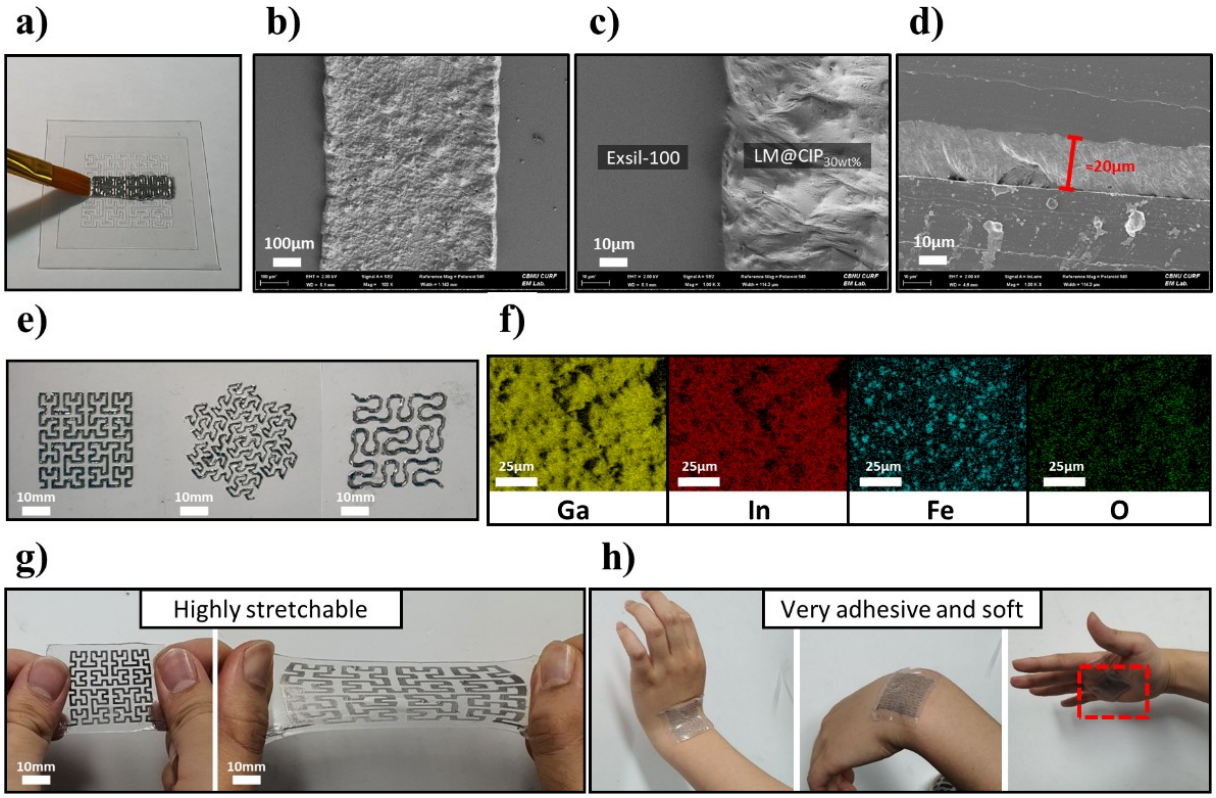

Figure 3: Morphological characterization of the LM@CIP wire patterned on the elastic substrate. (a) Photograph showing the LM@CIP wire patterned through the stencil on the elastic 100 substrate. (b,c,d) SEM images showing the (b) LM@CIP wire surface (c) LM@CIP wire surface with a higher magnification, (d) and cross-sectional view of the LM@CIP wire. (e) Three different fractal patterns of the LM@CIP wires. (f) Elemental analysis (Ga, In, Fe, and O) of the LM@CIP wire. (g, h) Photographs showing the stretchable, adhesive, and soft elastic devices patterned with the LM@CIP wires.

Figure 3a shows the fabrication process for WEDs patterned with LM@CIP directly on an elastic substrate via forced wetting through a stencil mask. The SEM image shows that LM@CIP is patterned through the stencil (Figure 3b), and the boundary between the elastic substrate and electrode is clearly visible (Figure 3c). As shown in Figure 3d, forced wetting creates a homogeneous 20 µm-thick LM@CIP wire on the elastic substrate. This facile approach to print fluidic electrode on elastic substrates also enables the formation of fractal patterns with various shapes (Figure 3d) which are mathematical space filling curves or architectures that can be customized to confine electrodes with longer lengths in small spaces [49]. As shown in the elemental analysis of the LM@CIP wire surface (Figure 3f), gallium and indium are mainly present with a certain amount of oxygen owing to the oxide layer on the LMW. Additionally, iron is detected uniformly throughout the surface, indicating that CIPs are well dispersed throughout the LM@CIP. The elastic devices patterned with LM@CIP wires preserve the soft(Young's modulus of 116 kPa), and stretchable (elongation at break of > 1300%) properties owing to the fluidic nature of the LM@CIP (Figure 3g and Figure S4). Additionally, the device adheres strongly to curved body surfaces because of the lower amount of silicone oil in the polymeric matrix of the non-crosslinked silicone elastomer used in this work (Figure 3h) [50].

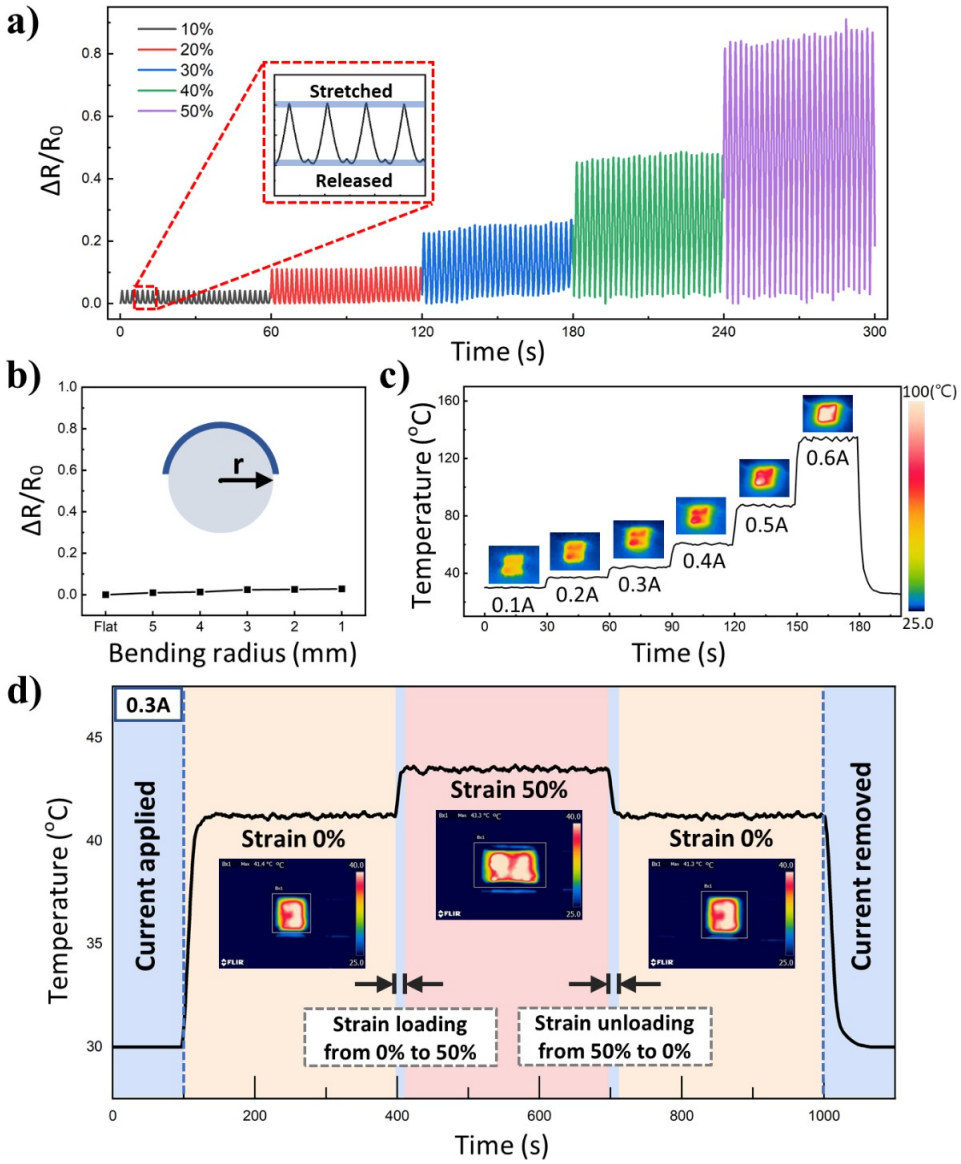

Figure 4: Characterizations of the thermal energy generated and relative resistance of the LMWs fractally patterned in the device. (a) Profile of the relative resistance of the LMWs for repeated strain cycles ranging from 10% to 50%. (b) Relative electrical resistance of the LMWs at different bending degrees. (c) Thermal profile of the LMWs upon applying various currents. (d) Thermal profile of the LMWs upon applying a 50% strain at a current of 0.3 A. Insets are infrared thermal images showing the temperature distribution during the loading and unloading of the strain while 0.3 A of current was applied.

Figure 4a shows the relative resistance changes of the LM@CIP wires fractally patterned in the devices during 30 cycles at various strains ranging from 10% to 50%. The resistance increases as a function of strain, but the LM@CIP wires exhibit a stable relative resistance response upon repeated tensile cycles. Figure 4b shows the changes in relative electrical resistance depending on the degree of device bending. The degree of bending changes from a flat state to a bending radius of 1 mm. With increase in bending radius, the relative resistance slightly increases by 0.03, indicating that the LM@CIP wire can preserve constant metallic

electrical conductivity to bending owing to highly deformable nature of the LM. Figure 4c shows that the temperature of the LM@CIP wire increases when the applied current is increased from 0.1 to 0.6 A in steps of 30 s. The inset infrared thermal images show the temperature as a function of the applied current. The fractally patterned LM@CIP wire increase temperatures to approximately 43 ˚C upon the application of 0.3 A current. We note this temperature range (40–45 ˚C) can potentially allow the devices to be used in thermotherapy [51] while the fractal-patterned LM@CIP wires generate thermal energy, reaching 135 ˚C upon a current application of 0.6 A. Figure 4d shows infrared thermal images of the fractal-patterned LM@CIP wires upon applying and removing a strain of 50%, while a current of 0.3 A was applied. The LM@CIP wires reach 41.4 ˚C upon applying a current of 0.3 A and reach 43.4 ˚C with a 50% strain. When the strain and current are removed, the LM@CIP wires rapidly recover the initial temperature owing to high thermal conductivity of the electrode.

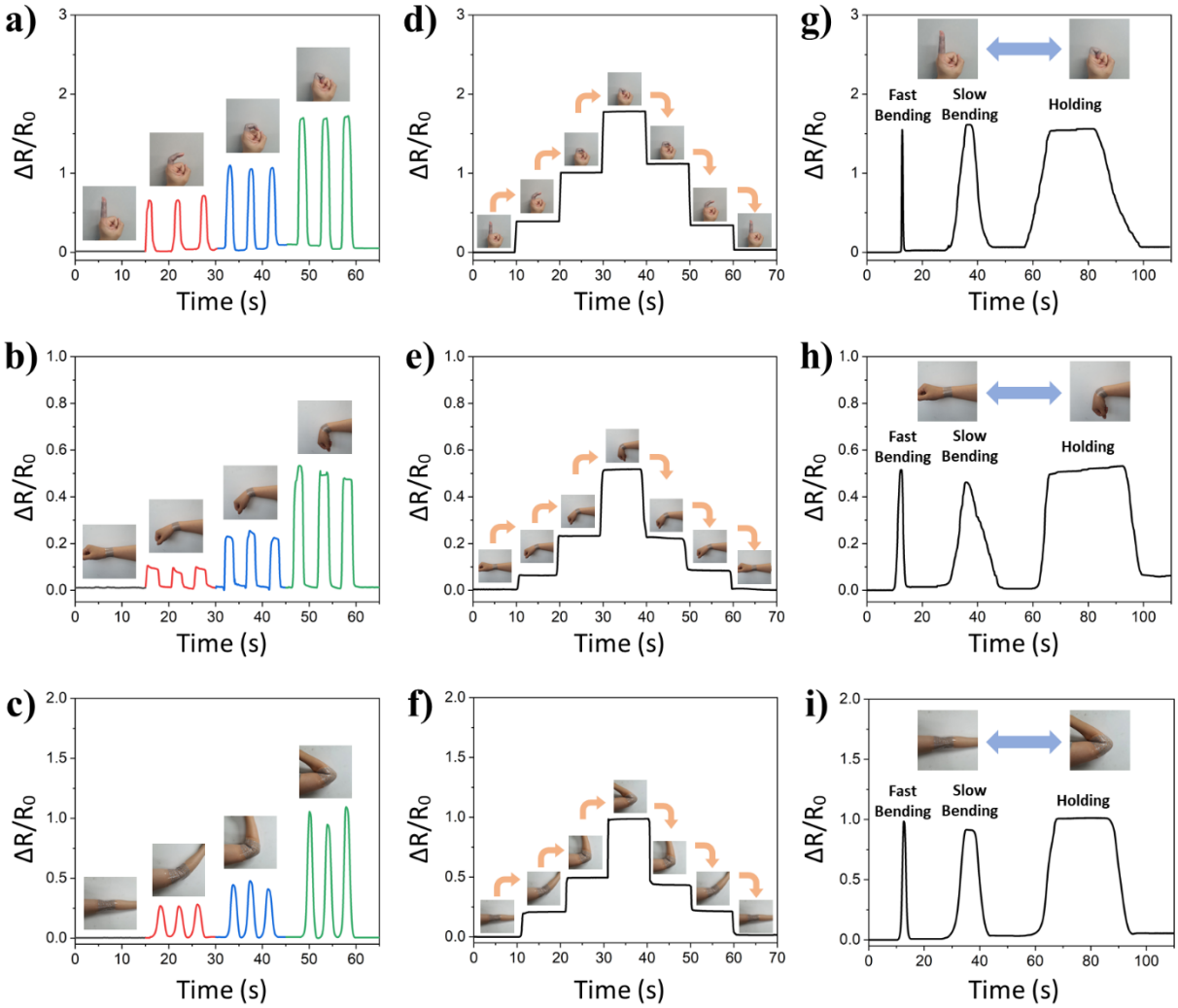

Figure 5: Wearable strain sensors used for monitoring various body motions. Relative resistance changes showing the sensor responses to bending and relaxing of (a)index finger (about 45°, 90°, and 180°), (b)wrist (about 30°, 45°, and 90°), and (c)elbow (about 45°, 90°, and 135°) with various degrees of bending. Relative resistance changes showing the sensor responses to stepwise bending and relaxing of (d) index finger (about

45°, 90°, and 180°), (e) wrist (about 30°, 45°, and 90°), and (f) elbow (about 45°, 90°, and 135°) for various degrees of bending. Relative resistance changes showing the sensor responses to different bending and relaxation rates on (g) index finger (about 180°), (h) wrist (about 90°), and (i) elbow (about 135°).

Figure 5 demonstrates that the elastic substrate patterned with the LMWs can be used as a wearable strain sensor to detect resistance changes upon strains. As the wearable sensors attached to the human body are strained by bending the index finger, wrist, and elbow, the relative electrical resistance changes. Figure 5a, b, and c show that the relative resistance of the device varies depending on the degree of bending while attached to the index finger (Figure 5a), wrist (Figure 5b), and elbow (Figure 5c), that is, a higher degree of bending leads to higher resistance changes. Figures 5d, e, and f show the stepwise changes of the relative resistance of the device attached to the index finger (Figure 5d), wrist (Figure 5e), and elbow (Figure 5f) over cycles of bending and relaxation. The degree of bending was fixed at each step and maintained for 10 s each. The relative resistance increases during the bending process with negligible changes in the resistance at a fixed state and the resistance gradually increases upon bending and decreases during relaxation. Figure 5g, h, and i show the relative resistance changes as a function of the bending rate while attached to the index finger (Figure 5g), wrist (Figure 5h), and elbow (Figure 5i). When the device attached to the joint is bent rapidly, a sharp peak with a sharp slope appears, whereas a wider range of relative resistance with a small slope appears for slow bending. When the bending state is maintained, the relative resistance is also constant at the highest value. These results demonstrate that the LMWs patterned soft devices can be utilized as wearable strain sensors to monitor bodily motions.

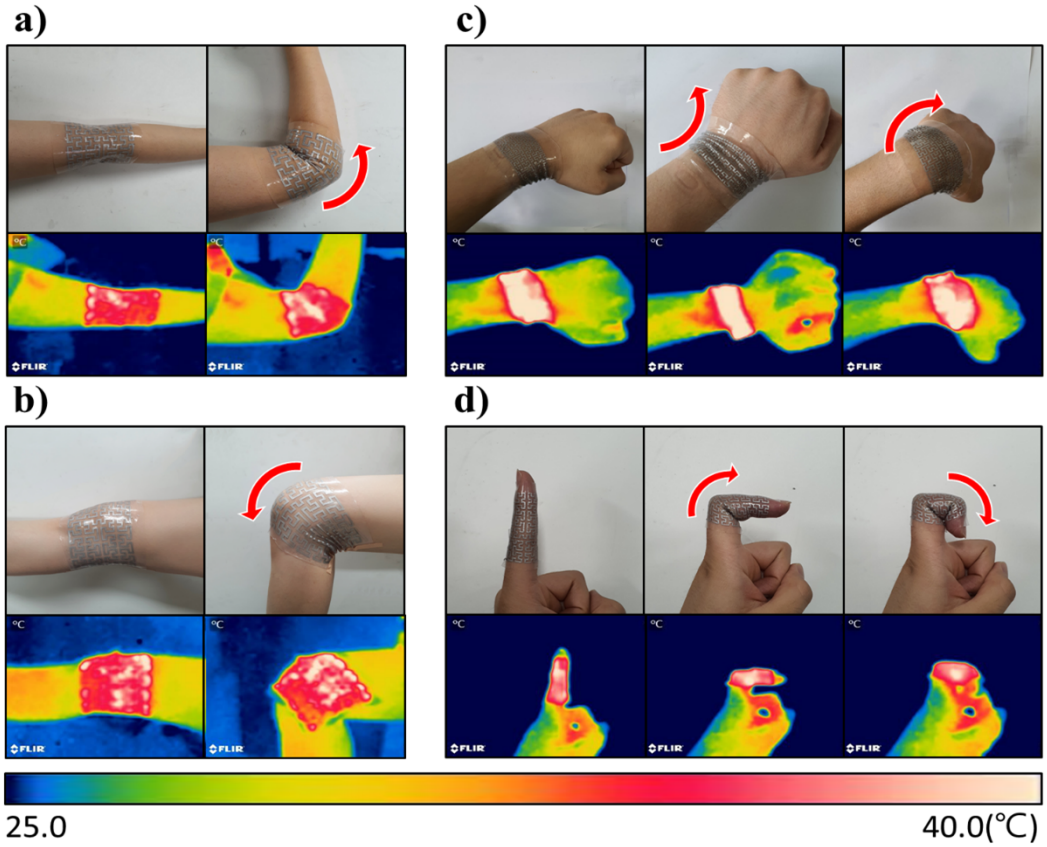

Figure 6: Photographs and infrared thermal images of wearable sensors patterned with LMWs attached on (a) the elbow, (b) knee, (c) wrist, and (d) index finger at various bending states.

Figure 6 shows photographs of the wearable strain sensors patterned with the LMWs attached to an elbow (Figure 6a), knee (Figure 6b), wrist (Figure 6c), and index finger (Figure 6d) upon applying various currents ranging from 0.2 to 0.8 A and the corresponding infrared thermal images with the joints in straight and bending states. The dimensions of the devices were customized according to the user and locations of attachment. The infrared thermal images show that the temperature of the LMWs was nearly constant after bending (Figure 6a and b), inverse bending (Figure 6c), and bending twice (Figure 6d) at approximately 90° on the joints. Therefore, the device exhibited dynamically stable thermal behavior, indicating significant advantages for application in wearable heating devices.

4. Conclusions

In summary, we developed stretchable and soft elastic devices that can be used as wearable polymeric heaters and strain sensors using LM@CIP electrodes patterned in the devices. The device was fabricated via forced wetting of the LM@CIP through dedicated stencils to pattern the electrode on elastic substrates. The resistance of the LMWs increased upon CIP addition, thereby enhancing the thermal energy generated via Joule heating through the LMWs, which can be increased as a function of the CIP content. The resulting heating performance was manipulated by geometrical factors, including the width and length of the electrodes. This soft and stretchable device patterned with LMWs can be mounted on joints owing to their strong adhesion to the surface and exhibit changes in relative resistance upon applying external strains. By utilizing this feature, the devices were used for wearable strain sensors to monitor various body motions. According to the results, the polymeric heaters and wearable strain sensors utilized LM electrodes would be used in soft robotics, electronic skin, and wearable health monitoring systems.

Acknowledgements

This work was supported by the National Research Foundation of Korea (NRF) grant funded by the Korean government (MSIT) (2021R1C1C1005083, RS-2023-00207836). Kunal Mondal gratefully acknowledges Oak Ridge National lab and the Department of Energy and Environment Science and Technology at the Idaho National Laboratory, USA, for their support.

References

[1] M. Kaur, T.H. Kim, W.S. Kim, New Frontiers in 3D Structural Sensing Robots, Adv. Mater. 33 (2021) 1–15. https://doi.org/10.1002/adma.202002534.

[2] G. Li, S. Liu, L. Wang, R. Zhu, Skin-inspired quadruple tactile sensors integrated on a robot hand enable object recognition, Sci. Robot. 5 (2020) 1–12. https://doi.org/10.1126/scirobotics.abc8134.

[3] E. Oh, T. Kim, J. Yoon, S. Lee, D. Kim, B. Lee, J. Byun, H. Cho, J. Ha, Y. Hong, Highly Reliable Liquid Metal–Solid Metal Contacts with a Corrugated Single-Walled Carbon Nanotube Diffusion Barrier for

Stretchable Electronics, Adv. Funct. Mater. 28 (2018) 1–11. https://doi.org/10.1002/adfm.201806014.

[4] Y. Zhao, S. Zhang, T. Yu, Y. Zhang, G. Ye, H. Cui, C. He, W. Jiang, Y. Zhai, C. Lu, X. Gu, N. Liu, Ultra-conformal skin electrodes with synergistically enhanced conductivity for long-time and low-motion artifact epidermal electrophysiology, Nat. Commun. 12 (2021) 1–12. https://doi.org/10.1038/s41467-021-25152-y.

[5] Y. Chen, S. Lu, S. Zhang, Y. Li, Z. Qu, Y. Chen, B. Lu, X. Wang, X. Feng, Skin-like biosensor system via electrochemical channels for noninvasive blood glucose monitoring, Sci. Adv. 3 (2017) 1–8. https://doi.org/10.1126/sciadv.1701629.

[6] J. Deng, H. Yuk, J. Wu, C.E. Varela, X. Chen, E.T. Roche, C.F. Guo, X. Zhao, Electrical bioadhesive interface for bioelectronics, Nat. Mater. 20 (2021) 229–236. https://doi.org/10.1038/s41563-020-00814-2.

[7] Y. He, Y. Zhao, L. Fan, X. Wang, M. Duan, H. Wang, X. Zhu, J. Liu, Injectable Affinity and Remote Magnetothermal Effects of Bi-Based Alloy for Long-Term Bone Defect Repair and Analgesia, Adv. Sci. 8 (2021) 1–11. https://doi.org/10.1002/advs.202100719.

[8] J. Chen, Y. Zhu, X. Chang, D. Pan, G. Song, Z. Guo, N. Naik, Recent Progress in Essential Functions of Soft Electronic Skin, Adv. Funct. Mater. 31 (2021) 1–34. https://doi.org/10.1002/adfm.202104686.

[9] S. Xiang, D. Liu, C. Jiang, W. Zhou, D. Ling, W. Zheng, X. Sun, X. Li, Y. Mao, C. Shan, Liquid-Metal-Based Dynamic Thermoregulating and Self-Powered Electronic Skin, Adv. Funct. Mater. 31 (2021) 1–10. https://doi.org/10.1002/adfm.202100940.

[10] S. Du, H. Suo, G. Xie, Q. Lyu, M. Mo, Z. Xie, N. Zhou, L. Zhang, J. Tao, J. Zhu, Self-powered and photothermal electronic skin patches for accelerating wound healing, Nano Energy. 93 (2022) 106906. https://doi.org/10.1016/j.nanoen.2021.106906.

[11] J. Cheng, J. Shang, S. Yang, J. Dou, X. Shi, X. Jiang, Wet-Adhesive Elastomer for Liquid Metal-Based Conformal Epidermal Electronics, Adv. Funct. Mater. 32 (2022) 1–12. https://doi.org/10.1002/adfm.202200444.

[12] K. Yamagishi, W. Zhou, T. Ching, S.Y. Huang, M. Hashimoto, Ultra-Deformable and Tissue-Adhesive Liquid Metal Antennas with High Wireless Powering Efficiency, Adv. Mater. 33 (2021) 1–15. https://doi.org/10.1002/adma.202008062.

[13] X. Ma, X. Li, W. Zhang, F. Meng, X. Wang, Y. Qin, M. Zhang, Carbon-based nanocomposite smart sensors for the rapid detection of mycotoxins, Nanomaterials. 11 (2021) 1–24. https://doi.org/10.3390/nano11112851.

[14] Y. Qin, J. Mo, Y. Liu, S. Zhang, J. Wang, Q. Fu, S. Wang, S. Nie, Stretchable Triboelectric Self-Powered Sweat Sensor Fabricated from Self-Healing Nanocellulose Hydrogels, Adv. Funct. Mater. 2201846 (2022) 2201846. https://doi.org/10.1002/adfm.202201846.

[15] Q. Su, Q. Zou, Y. Li, Y. Chen, S.Y. Teng, J.T. Kelleher, R. Nith, P. Cheng, N. Li, W. Liu, S. Dai, Y. Liu, A. Mazursky, J. Xu, L. Jin, P. Lopes, S. Wang, A stretchable and strain-unperturbed pressure sensor for motion interference-free tactile monitoring on skins, Sci. Adv. 7 (2021). https://doi.org/10.1126/sciadv.abi4563.

[16] M.G. Saborio, S. Cai, J. Tang, M.B. Ghasemian, M. Mayyas, J. Han, M.J. Christoe, S. Peng, P. Koshy, D. Esrafilzadeh, R. Jalili, C.H. Wang, K. Kalantar-Zadeh, Liquid Metal Droplet and Graphene Co-Fillers for Electrically Conductive Flexible Composites, Small. 16 (2020) 1–12. https://doi.org/10.1002/smll.201903753.

[17] R. Tutika, A.B.M.T. Haque, M.D. Bartlett, Self-healing liquid metal composite for reconfigurable and recyclable soft electronics, Commun. Mater. 2 (2021) 1–8. https://doi.org/10.1038/s43246-021-00169-4.

[18] C.J. Thrasher, Z.J. Farrell, N.J. Morris, C.L. Willey, C.E. Tabor, Mechanoresponsive Polymerized Liquid Metal Networks, Adv. Mater. 31 (2019) 1–8. https://doi.org/10.1002/adma.201903864.

[19] S. Choi, J. Park, W. Hyun, J. Kim, J. Kim, Y.B. Lee, C. Song, H.J. Hwang, J.H. Kim, T. Hyeon, D.H. Kim, Stretchable Heater Using Ligand-Exchanged Silver Nanowire Nanocomposite for Wearable Articular Thermotherapy, ACS Nano. 9 (2015) 6626–6633. https://doi.org/10.1021/acsnano.5b02790.

[20] H. Kim, M. Seo, J.W. Kim, D.K. Kwon, S.E. Choi, J.W. Kim, J.M. Myoung, Highly Stretchable and Wearable Thermotherapy Pad with Micropatterned Thermochromic Display Based on Ag Nanowire–Single-Walled Carbon Nanotube Composite, Adv. Funct. Mater. 29 (2019) 1–11. https://doi.org/10.1002/adfm.201901061.

[21] S. Hong, H. Lee, J. Lee, J. Kwon, S. Han, Y.D. Suh, H. Cho, J. Shin, J. Yeo, S.H. Ko, Highly Stretchable and Transparent Metal Nanowire Heater for Wearable Electronics Applications, Adv. Mater. 27 (2015) 4744–4751. https://doi.org/10.1002/adma.201500917.

[22] M. Zhang, C. Wang, X. Liang, Z. Yin, K. Xia, H. Wang, M. Jian, Y. Zhang, Weft-Knitted Fabric for a Highly Stretchable and Low-Voltage Wearable Heater, Adv. Electron. Mater. 3 (2017) 1–8. https://doi.org/10.1002/aelm.201700193.

[23] D. Kong, Y. Li, S. Feng, S. Cao, J. Zhang, Printable liquid metal microparticle ink for ultrastretchable electronics, ACS Appl. Mater. Interfaces. (2020). https://doi.org/10.1021/acsami.0c15084.

[24] M. Saito, E. Kanai, H. Fujita, T. Aso, N. Matsutani, T. Fujie, Flexible Induction Heater Based on the Polymeric Thin Film for Local Thermotherapy, Adv. Funct. Mater. 31 (2021) 1–9. https://doi.org/10.1002/adfm.202102444.

[25] R. Wang, Z. Xu, J. Zhuang, Z. Liu, L. Peng, Z. Li, Y. Liu, W. Gao, C. Gao, Highly Stretchable Graphene Fibers with Ultrafast Electrothermal Response for Low-Voltage Wearable Heaters, Adv. Electron. Mater. 3 (2017). https://doi.org/10.1002/aelm.201600425.

[26] B.W. An, E.J. Gwak, K. Kim, Y.C. Kim, J. Jang, J.Y. Kim, J.U. Park, Stretchable, Transparent Electrodes as Wearable Heaters Using Nanotrough Networks of Metallic Glasses with Superior Mechanical Properties and Thermal Stability, Nano Lett. 16 (2016) 471–478. https://doi.org/10.1021/acs.nanolett.5b04134.

[27] J. Zhou, M. Mulle, Y. Zhang, X. Xu, E.Q. Li, F. Han, S.T. Thoroddsen, G. Lubineau, High-ampacity conductive polymer microfibers as fast response wearable heaters and electromechanical actuators, J. Mater. Chem. C. 4 (2016) 1238–1249. https://doi.org/10.1039/c5tc03380b.

[28] M.D. Dickey, R.C. Chiechi, R.J. Larsen, E.A. Weiss, D.A. Weitz, G.M. Whitesides, Eutectic gallium-indium (EGaIn): A liquid metal alloy for the formation of stable structures in microchannels at room temperature, Adv. Funct. Mater. 18 (2008) 1097–1104. https://doi.org/10.1002/adfm.200701216.

[29] M.D. Dickey, Stretchable and Soft Electronics using Liquid Metals, Adv. Mater. 29 (2017) 1–19. https://doi.org/10.1002/adma.201606425.

[30] P. Won, S. Jeong, C. Majidi, S.H. Ko, Recent advances in liquid-metal-based wearable electronics and materials, IScience. 24 (2021) 102698. https://doi.org/10.1016/j.isci.2021.102698.

[31] M.G. Mohammed, R. Kramer, All-Printed Flexible and Stretchable Electronics, Adv. Mater. 29 (2017). https://doi.org/10.1002/adma.201604965.

[32] Y. Lin, O. Gordon, M.R. Khan, N. Vasquez, J. Genzer, M.D. Dickey, Vacuum filling of complex microchannels with liquid metal, Lab Chip. 17 (2017) 3043–3050. https://doi.org/10.1039/c7lc00426e.

[33] S. Liu, M.C. Yuen, E.L. White, J.W. Boley, B. Deng, G.J. Cheng, R. Kramer-Bottiglio, Laser Sintering of Liquid Metal Nanoparticles for Scalable Manufacturing of Soft and Flexible Electronics, ACS Appl. Mater. Interfaces. 10 (2018) 28232–28241. https://doi.org/10.1021/acsami.8b08722.

[34] T. Lu, L. Finkenauer, J. Wissman, C. Majidi, Rapid prototyping for soft-matter electronics, Adv. Funct. Mater. 24 (2014) 3351–3356. https://doi.org/10.1002/adfm.201303732.

[35] T. V. Neumann, E.G. Facchine, B. Leonardo, S. Khan, M.D. Dickey, Direct write printing of a self-encapsulating liquid metal-silicone composite, Soft Matter. 16 (2020) 6608–6618. https://doi.org/10.1039/d0sm00803f.

[36] C. Ladd, J.H. So, J. Muth, M.D. Dickey, 3D printing of free standing liquid metal microstructures, Adv. Mater. 25 (2013) 5081–5085. https://doi.org/10.1002/adma.201301400.

[37] P. Bhuyan, D. Cho, M. Choe, S. Lee, S. Park, Liquid Metal Patterned Stretchable and Soft Capacitive Sensor with Enhanced Dielectric Property Enabled by Graphite Nanofiber Fillers, Polymers (Basel). 14 (2022). https://doi.org/10.3390/polym14040710.

[38] D. Cho, P. Bhuyan, D. Sin, H. Kim, E. Kim, S. Park, Stretchable, Soft, and Variable Stiffness Elastomer foam with Positive and Negative Piezoresistivity Enabled by Liquid Metal Inclusion, Adv. Mater. Technol. 7 (2022) 1–9. https://doi.org/10.1002/admt.202101092.

[39] D. Sin, V.K. Singh, P. Bhuyan, Y. Wei, H.M. Lee, B.J. Kim, S. Park, Ultrastretchable Thermo- and Mechanochromic Fiber with Healable Metallic Conductivity, Adv. Electron. Mater. 7 (2021) 1–8. https://doi.org/10.1002/aelm.202100146.

[40] Y. Jin, Y. Lin, A. Kiani, I.D. Joshipura, M. Ge, M.D. Dickey, Materials tactile logic via innervated soft thermochromic elastomers, Nat. Commun. 10 (2019) 1–8. https://doi.org/10.1038/s41467-019-12161-1.

[41] H. Wang, W. Xing, S. Chen, C. Song, M.D. Dickey, T. Deng, Liquid Metal Composites with Enhanced Thermal Conductivity and Stability Using Molecular Thermal Linker, Adv. Mater. 33 (2021) 1–11. https://doi.org/10.1002/adma.202103104.

[42] H. Chang, P. Zhang, R. Guo, Y. Cui, Y. Hou, Z. Sun, W. Rao, Recoverable Liquid Metal Paste with Reversible Rheological Characteristic for Electronics Printing, ACS Appl. Mater. Interfaces. 12 (2020) 14125–14135. https://doi.org/10.1021/acsami.9b20430.

[43] R. Zhou, P. Li, Z. Fan, D. Du, J. Ouyang, Stretchable heaters with composites of an intrinsically conductive polymer, reduced graphene oxide and an elastomer for wearable thermotherapy, J. Mater. Chem. C. 5 (2017) 1544–1551. https://doi.org/10.1039/c6tc04849h.

[44] Z. Yang, W. Wang, L. Bi, L. Chen, G. Wang, G. Chen, based on a multifunctional PET / silver, (2020) 16562–16569. https://doi.org/10.1039/d0nr04023a.

[45] H. Zhai, R. Wang, X. Wang, Y. Cheng, L. Shi, J. Sun, Transparent heaters based on highly stable Cu nanowire, 1 (2016) 1–13. https://doi.org/10.1007/s12274-016-1261-0.

[46] Y. Cheng, H. Zhang, R. Wang, X. Wang, H. Zhai, T. Wang, Q. Jin, J. Sun, Highly Stretchable and Conductive Copper Nanowire Based Fibers with Hierarchical Structure for Wearable Heaters, (2016). https://doi.org/10.1021/acsami.6b09293.

[47] K. Hong, M. Choe, S. Kim, H.M. Lee, B.J. Kim, S. Park, An ultrastretchable electrical switch fiber with a magnetic liquid metal core for remote magnetic actuation, Polymers (Basel). 13 (2021). https://doi.org/10.3390/polym13152407.

[48] S. Kim, S. Kim, K. Hong, M.D. Dickey, S. Park, Liquid-Metal-Coated Magnetic Particles toward Writable , Nonwettable , Stretchable Circuit Boards , and Directly Assembled Liquid Metal-Elastomer Conductors, (2022). https://doi.org/10.1021/acsami.2c07618.

[49] J.A. Fan, W.H. Yeo, Y. Su, Y. Hattori, W. Lee, S.Y. Jung, Y. Zhang, Z. Liu, H. Cheng, L. Falgout, M. Bajema, T. Coleman, D. Gregoire, R.J. Larsen, Y. Huang, J.A. Rogers, Fractal design concepts for stretchable electronics, Nat. Commun. 5 (2014) 1–8. https://doi.org/10.1038/ncomms4266.

[50] P. Bhuyan, Y. Wei, D. Cho, U.T. Nakate, S. Kim, S. Lee, M. Choe, H. Jeon, S. Park, Multifunctional ultrastretchable and ultrasoft electronics enabled by uncrosslinked polysiloxane elastomers patterned with rheologically modified liquid metal electrodes : Beyond current soft and stretchable electronics, Chem. Eng. J. 453 (2023) 139832. https://doi.org/10.1016/j.cej.2022.139832.

[51] C.M. Bleakley, J.T. Costello, Do thermal agents affect range of movement and mechanical properties in soft tissues? A systematic review, Arch. Phys. Med. Rehabil. 94 (2013) 149–163. https://doi.org/10.1016/j.apmr.2012.07.023.